

Electronic Supplementary Information

From Angular to Round: In Depth Interfacial Analysis of Binary Phosphatidylethanolamine Mixtures in the Inverse Hexagonal Phase

Gerome Vancuylenberg, Amin Sadeghpour, Arwen Tyler and Michael Rappolt*

School of Food Science and Nutrition, University of Leeds, UK.

**E-mail: m.rappolt@leeds.ac.uk*

Contents

Fig. S1 Fitting of the diffraction pattern.	2
Fig. S2 Best phase choices for F(21), F(22) and F(31)	3
Fig. S3 Schematic of the encasing triangle used in circumference and area calculation	4
Fig. S4 Peak-shape progression in $\langle 10 \rangle$ and $\langle 11 \rangle$ direction and MCT fits.	5
Fig. S5 Fraction of the inverse hexagonal phase as function of the DPPE concentration.	6
Table S1 Structural parameters for the calculation of the electron density maps.	7
Fig. S6 Electron density maps of all POPE/DPPE mixtures as function of mol% DPPE.	8
Fig. S7 Electron density fluctuation along the head-group and methyl trough interface.	9
Fig. S8 Radial electron density profiles with orientation of $\gamma = 0^\circ$ and $\gamma = 30^\circ$.	10
Fig. S9 Free energy, bending energy and stretching energy per lipid.	11
Reference	12

Fitting of the diffraction pattern

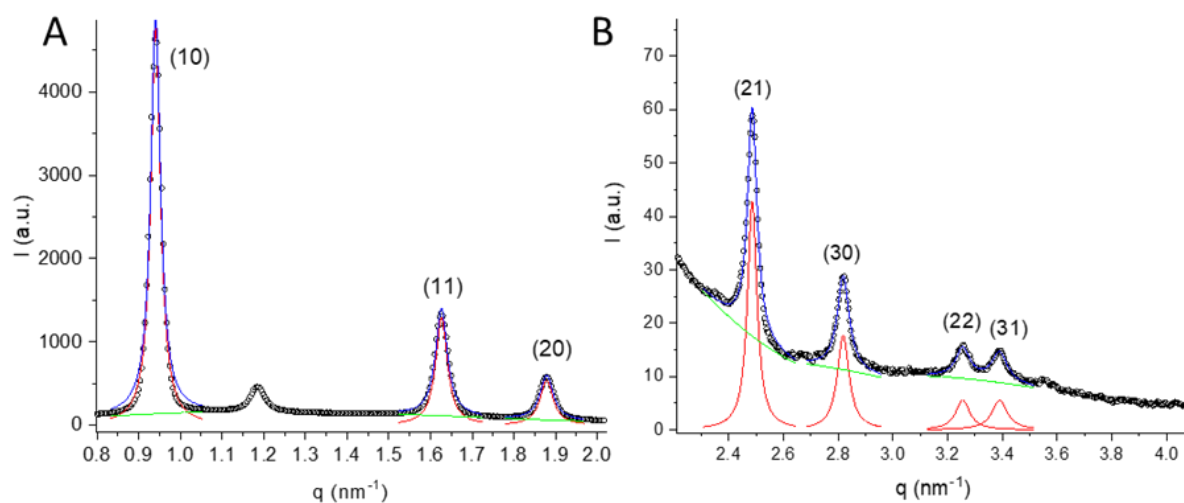


Fig. S1 SAXS diffraction pattern of POPE with 12 mol% of DPPE. (A) Higher intensity peaks (10), (11) and (20) are shown, and in (B), the lower intensity peaks (21), (30), (22) and (31) are displayed. All peaks are fitted by Lorentzian distributions (red-lines), the diffuse background was fitted with a polynomial of second order (green lines) and the overall resulting fits are shown with blue lines. All experimental results are summarized Table S1.

Best phase choices for F(21), F(22) and F(31)

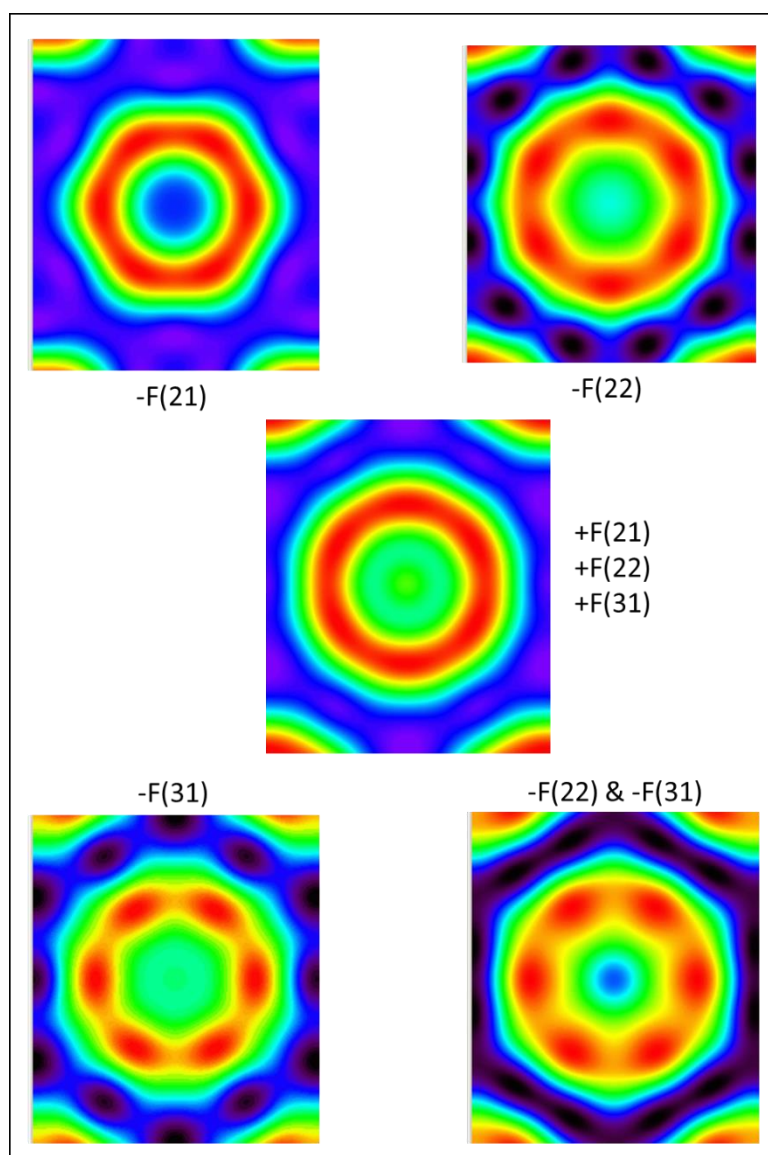


Fig. S2 Demonstration of best phase combination for the POPE sample with 9 mol% of DPPE. Due to experimentally reported zero-crossing of the form factor near the (21) reflection¹, its best phase choice has been checked for all electron density map calculations. Additionally, the two weakest reflections (22) and (31) reflections were checked for their best phase choices. All these alternative phase choices led to an enhanced kurtosis (peakedness) within the unit cell and hence have been excluded. This phase choice method has been originally developed by Luzzati and co-workers², and follows the idea to identify electron density map, displaying the smoothest interfaces. Moreover, the best phase choice for F(21), F(22) and F(31) (all positive), leads also to the lipid/water interface with the highest circularity.

Schematic of the encasing triangle used in circumference and area calculation

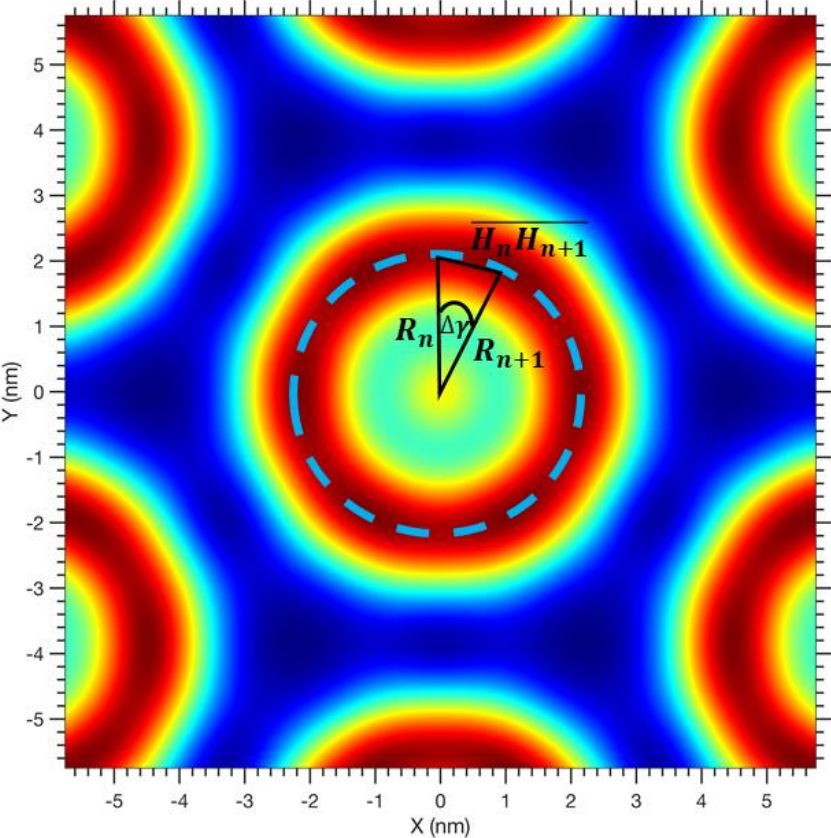


Fig. S3 Schematic representation method used to calculate the circumference and area of the water core, with the phosphate position denoted by the light blue dotted line. $\Delta\gamma$ was set at 1° . The summation $\sum_{n=0}^{n=30} \overline{H_n H_{n+1}}$ produces the approximate arch length of a 30° segment with the area of the encasing triangle used to calculate the total area of the water core (note, $\Delta\gamma$ is not to scale).

Peak-shape progression in <10> and <11> direction and MCT fits

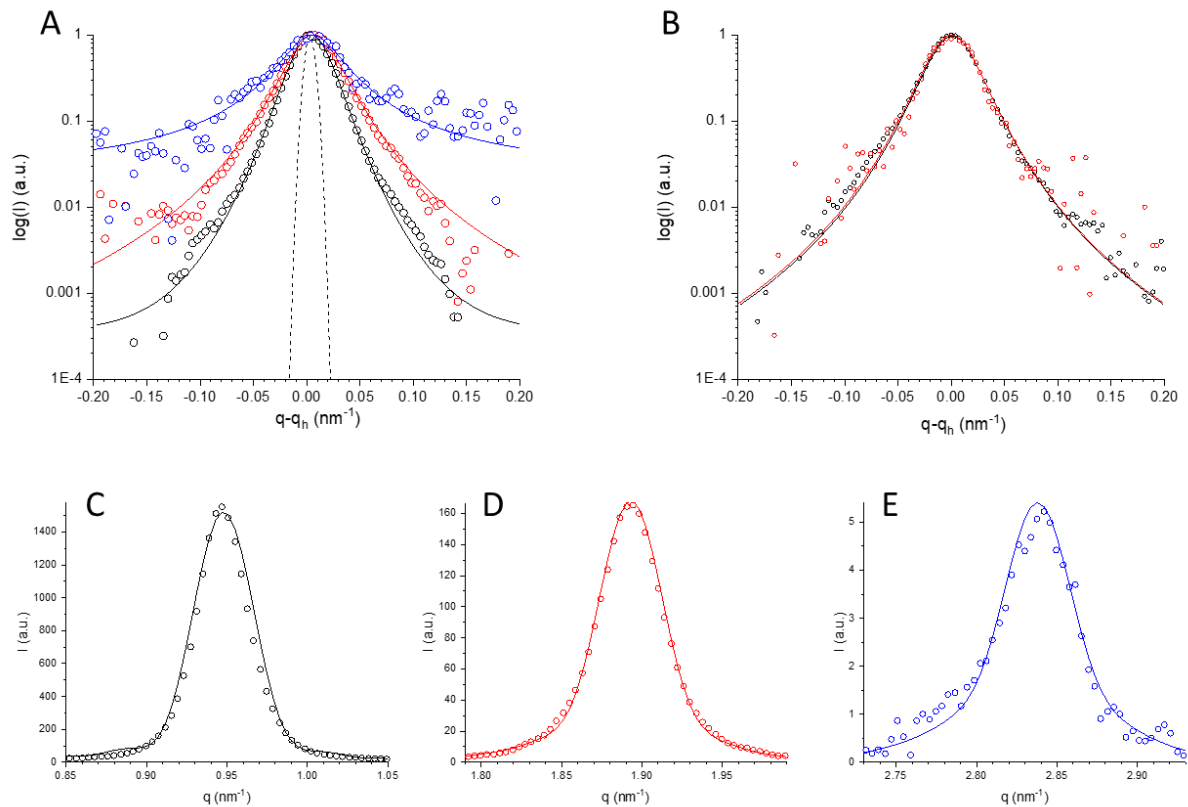


Fig. S4 (A) The peak shape progression in the <10> direction shows an increase in width as function of the order (peak (10) – black, (20) – red, (30) – blue, instrumental width – dashed line), which demonstrates disorder of 2nd kind with strong undulations within this set of planes. (B) The peak shape progression in the <11> direction displays a constant width as function of the order (peak (11) – black, (11) – red), which demonstrates dominating thermal disorder instead (all lines in panel A and B display Pearson VII fits, helping to guide the eye). (C-D) Modified Caillé Theory based fits in the <10> direction: from left to right the (10), (20) and (30) peaks were fitted, resulting mean square fluctuations $\sigma = 0.3$ nm. As an example, the sample POPE with 9 mol% DPPE is presented.

Turnover curves: L_α to H_{II} phase transition

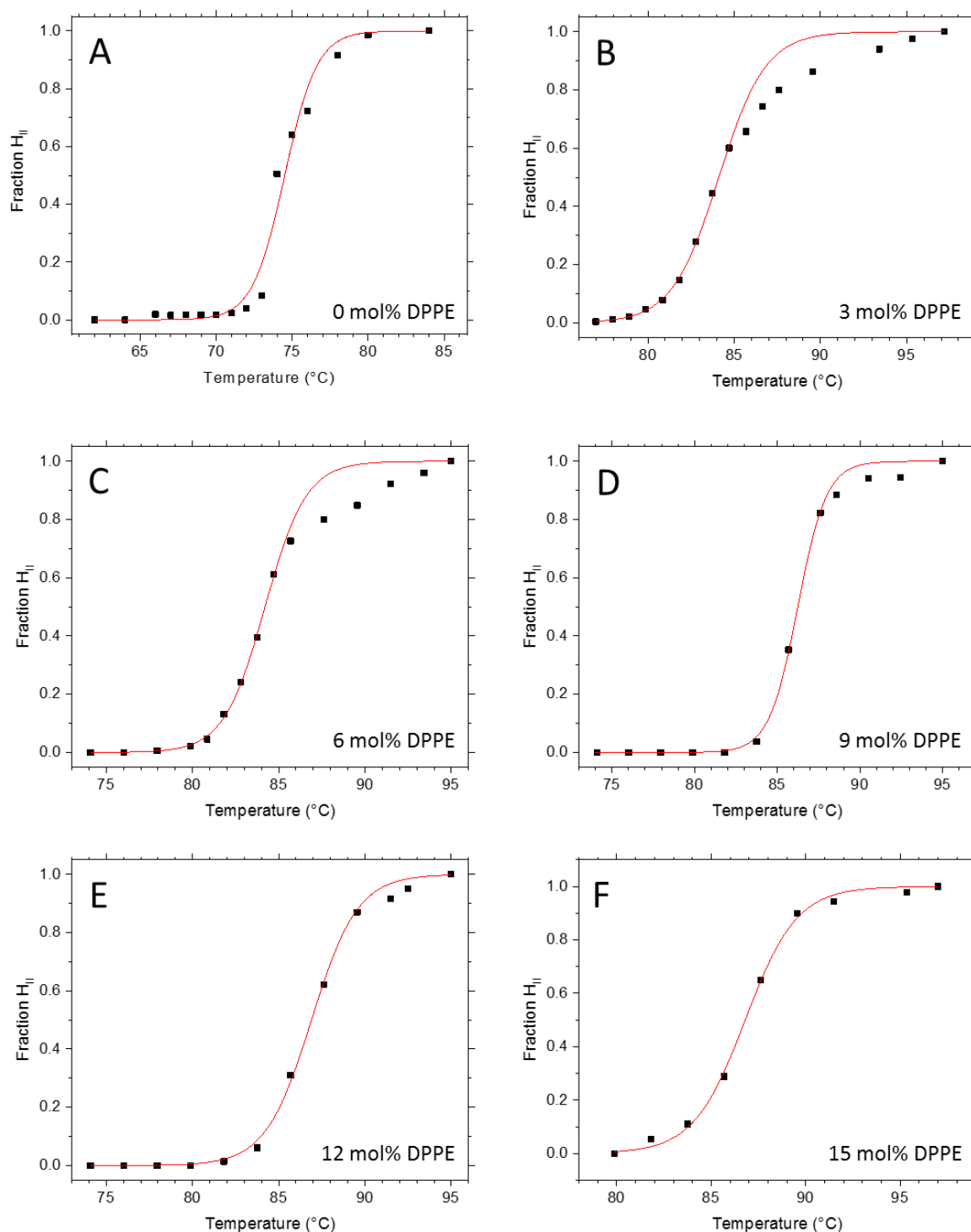


Fig. S5 Fraction of the inverse hexagonal phase as function of the DPPE concentration. Mixtures of POPE/DPPE ranging from 0 to 15 mol% DPPE were heated from L_α to H_{II} phase. The intensity of the first order peaks was used to calculate the fraction of the inverse hexagonal phase according to $Fraction\ H_{II} = I(H_{II})/[I(H_{II}) + I(L_\alpha)]$. Best fits using the logistic function with setting the minimum and maximum values to 0 and 1, respectively, are shown in red. Panel A data is taken from Rappolt et al.³

Table S1 Structural parameters for the calculation of the electron density maps in Fig. S5.

Sample	Temperature (°C)	Lattice spacing, <i>a</i> (nm)	Miller indexes: <i>h, k</i>	I_{hk}/I_{10} ^a	$F_{h,k}/F_{10}$ ^b
0 mol% DPPE	80.0	7.12	1, 0	1.0000	+1.00
			1, 1	0.3608	-1.04
			2, 0	0.1752	-0.84
			2, 1	0.0069	+0.22
			3, 0	0.0058	+0.23
			2, 2	0.0036	+0.21
			3, 1	0.0019	+0.16
3 mol% DPPE	89.5	7.66	1, 0	1.0000	+1.00
			1, 1	0.3168	-0.97
			2, 0	0.1457	-0.76
			2, 1	0.0054	+0.19
			3, 0	0.0058	+0.23
			2, 2	0.0028	+0.18
			3, 1	0.0015	+0.14
6 mol% DPPE	89.5	7.73	1, 0	1.0000	+1.00
			1, 1	0.3376	-1.01
			2, 0	0.1540	-0.78
			2, 1	0.0066	+0.22
			3, 0	0.0072	+0.26
			2, 2	0.0018	+0.15
			3, 1	0.0011	+0.12
9 mol% DPPE	90.5	7.66	1, 0	1.0000	+1.00
			1, 1	0.3265	-0.99
			2, 0	0.1544	-0.79
			2, 1	0.0060	+0.20
			3, 0	0.0070	+0.25
			2, 2	0.0020	+0.15
			3, 1	0.0013	+0.13
12 mol% DPPE	91.5	7.72	1, 0	1.0000	+1.00
			1, 1	0.3319	-1.00
			2, 0	0.1548	-0.79
			2, 1	0.0068	+0.22
			3, 0	0.0061	+0.23
			2, 2	0.0029	+0.19
			3, 1	0.0012	+0.12
15 mol% DPPE	91.5	7.70	1, 0	1.0000	+1.00
			1, 1	0.3201	-0.98
			2, 0	0.1521	-0.78
			2, 1	0.0063	+0.21
			3, 0	0.0059	+0.23
			2, 2	0.0027	+0.18
			3, 1	0.0011	+0.12

^a All I_{21} and I_{31} intensities were divided by 2 due to their 2-fold higher multiplicity.

^b Amplitudes $F_{hk}/F_{10} = \sqrt{(I_{hk}/I_{10}) Lor_c}$, i.e., the Lorentz correction (Lor_c) was 1, $\sqrt{3}$, 2, $\sqrt{7}$, 3, $\sqrt{12}$ and $\sqrt{13}$ applied.

Electron density maps of POPE/DPPE mixtures

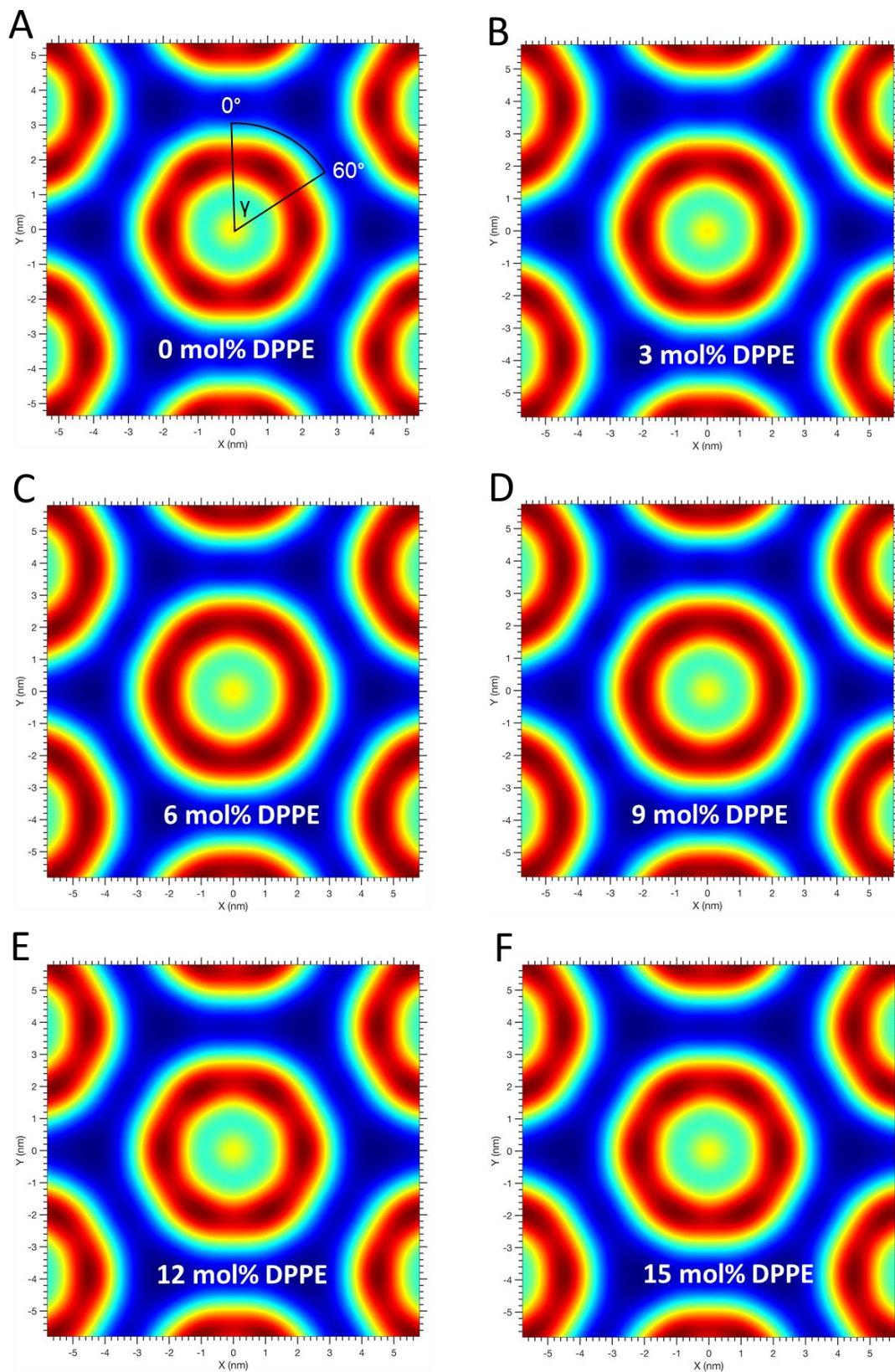


Fig. S6 Electron density maps of all POPE/DPPE mixtures as function of mol% DPPE. All experimental conditions and parameters are summarized in Table S1.

Interfacial electron density fluctuation

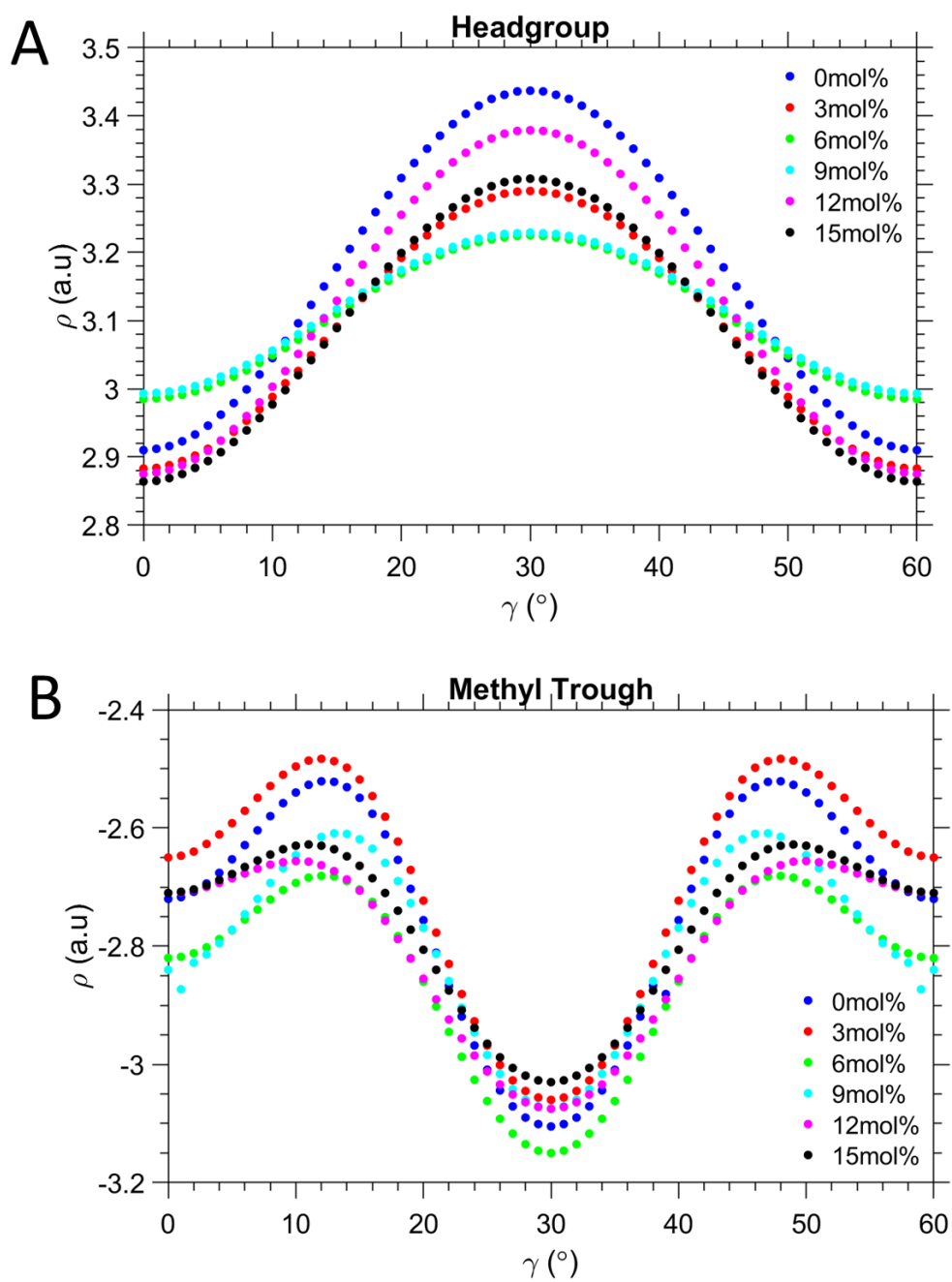


Fig. S7 Electron density fluctuation along the head-group (A) and methyl trough interfaces (B). Note, these interfaces are defined in Fig. 3A.

Radial electron density profiles

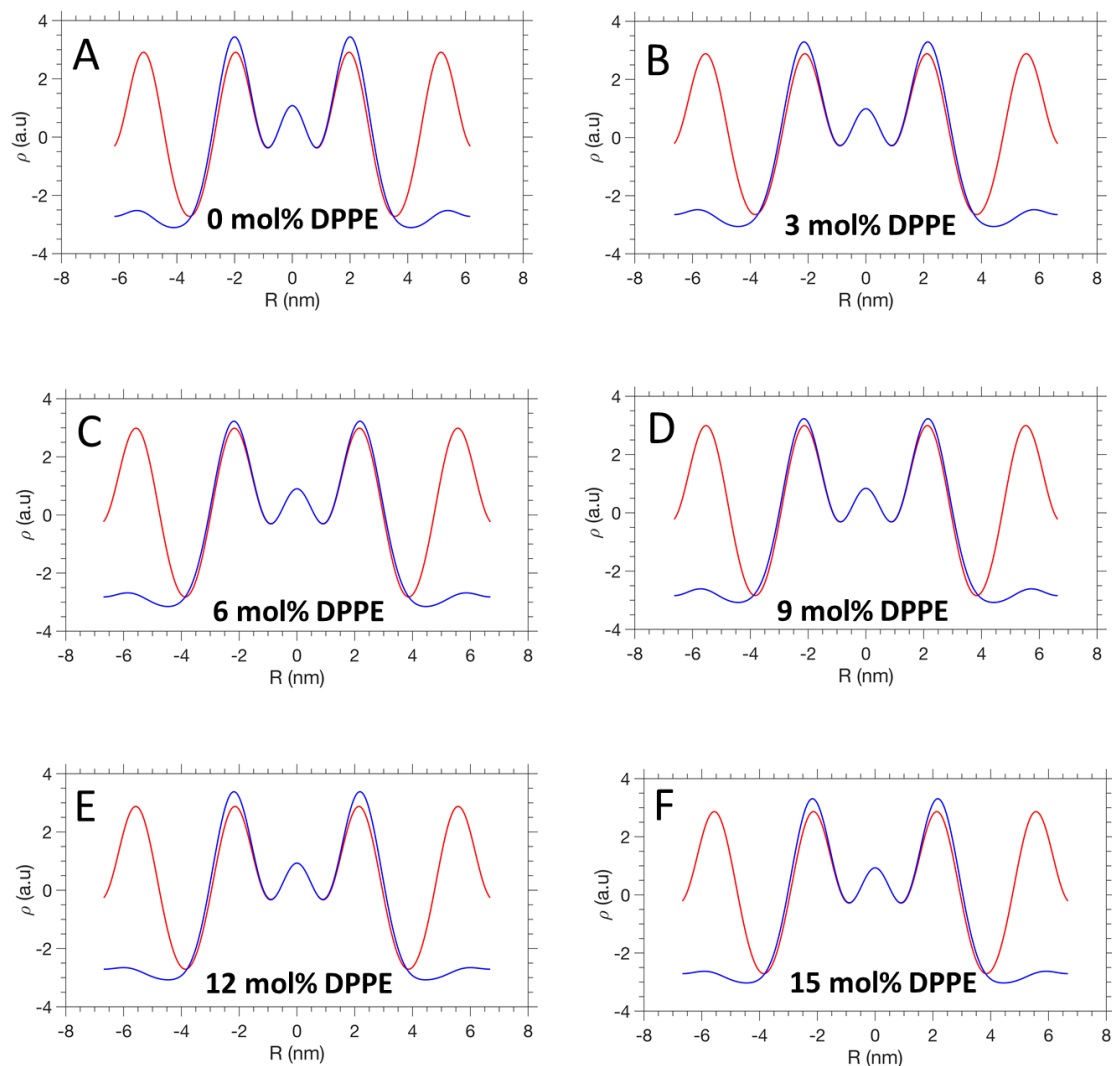


Fig. S8 Radial electron density profiles with orientation of $\gamma = 0^\circ$ (red) and $\gamma = 30^\circ$ (blue). Note, γ orientations are defined in Fig. S2 A.

Free energy, bending energy and stretching energy per lipid

In the derivation of the free energy of lipid monolayers, Iglič and colleagues⁴ assume that lipid molecules are **anisotropic in shape** in the inverse hexagonal phase (see molecular wedge model in Figure 1B) with respect to the axis perpendicular to the membrane plane. In their model for the lipid monolayer free energy two energy contributions are considered: the bending energy, which involves also a **deviatoric curvature term**, D , which is an additional term to the mean curvature, H , and second, the interstitial energy, which describes the deformation energy due to stretching of the phospholipid molecule chains. Note, that the classic description of the bending energy of monolayers assumes only molecular shapes with axis rotational symmetry, which has been shown to oversimplify the description of bending energies in the inverse hexagonal phase (see also references^{5, 6}). On the basis of the derived expression for the lipid monolayer free energy (equation 58 in reference⁴), the authors predict optimal geometry and physical conditions for the stability of the inverted hexagonal phase.

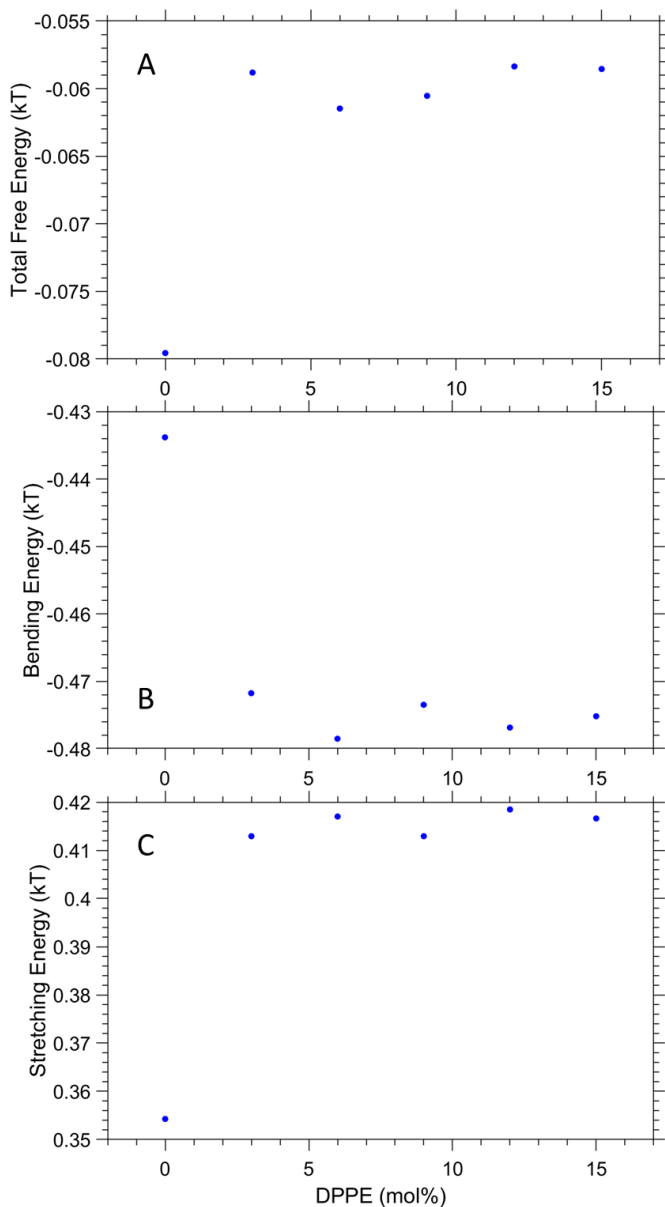


Fig. S9 Free energy, bending energy and stretching energy per lipid following the theory of Aleš Iglič and colleagues⁴ with the stretching modulus $\tau = 13.5$ kT, the bending modulus $K_C = 11$ kT, the mean curvature $H = -1/(R_{p\ ave} + 0.5 D_H)$ nm⁻¹ with the headgroup extension $D_H = 1.1$ nm, the deviatoric curvature $D = |H|$, the intrinsic mean curvature $H_m = 0.1$ nm⁻¹, the intrinsic deviatoric curvature $D_m = |H_m|$, the chain length, $d_C = l_{ave} - D_H/2$ and the area per lipid at the polar/apolar interface, $A_N = A_P (R_{p\ ave} + 0.5 D_H)/R_{p\ ave}$. Best estimations of the model constants for POPE (given in bold above) were taken literature⁴, all other parameters were derived from $R_{p\ ave}$ and A_P values from this study (see Table 1).

Reference

1. D. C. Turner and S. M. Gruner, *Biochemistry*, 1992, **31**, 1340-1355.
2. P. Mariani, V. Luzzati and H. Delacroix, *J.Mol.Biol.*, 1988, **204**, 165-189.
3. M. Rappolt, A. Hickel, F. Bringezu and K. Lohner, *Biophysical Journal*, 2003, **84**, 3111-3122.
4. S. Perutkova, M. Daniel, G. Dolinar, M. Rappolt, V. Kralj-Iglic and A. Iglic, in *Advances in Planar Lipid Bilayers and Liposomes*, eds. A. Leitmannova-Liu and H. T. Tien, Elsevier, Academic Press, Burlington, 2009, vol. 9, pp. 238-278.
5. T. Mareš, M. Daniel, Š. Perutkova, A. Perne, G. Dolinar, A. Iglíč, M. Rappolt and V. Kralj-Iglič, *J. Phys. Chem. B*, 2008, **112**, 16575-16584.
6. S. Perutkova, M. Daniel, M. Rappolt, G. Pabst, G. Dolinar, V. Kralj-Iglic and A. Iglic, *Phys.Chem.Chem.Phys.*, 2011, **13**, 3100-3107.